# Wide-Band $S$-Parameter Extraction From FD-TD Simulations for Propagating and Evanescent Modes in Inhomogeneous Guides

Wojciech K. Gwarek, *Fellow, IEEE,* and Malgorzata Celuch-Marcysiak, *Member, IEEE*

***Abstract*—This paper proposes a new method of $S$-parameter extraction from finite-difference time-domain simulations. Unlike the previously published methods, the present method extracts the frequency-dependent mode impedance and propagation constant directly from the three-dimensional simulations. This makes it accurate and computationally effective in wide-band analysis. This paper provides examples of calculations including difficult cases of inhomogeneous or lossy structures, with the frequency band spanning below and above the cutoff frequency. Special attention is given to the $S$-parameter extraction for evanescent modes. It is shown that the available literature provides insufficient and sometimes confusing background in this regard. Thus, a new consistent theoretical background is presented.**

***Index Terms*—Circuit simulation, computer-aided analysis, electromagnetic analysis, scattering parameters.**

## I. Introduction

$S$-PARAMETER extraction from finite-difference time-domain (FD-TD) simulations of microwave circuits has been considered by many authors. Originally, the interest was concentrated on propagating modes, assumed to be perfectly matched at ports (e.g., [1]). Due to problems with wide-band modeling of well-matched ports, more general methods allowing for a controlled mismatch have been further proposed [2]–[5]. However, extensions to evanescent modes have been scarce and practically limited to homogeneous waveguides.

Let us note that evanescent modes at ports are also of great practical interest in a wide range of applications. Moreover, the most effective way of the analysis can often be obtained by circuit segmentation [6] and by calculating different segments separately, by either applying the same method or even applying different simulation methods to different segments. As an example, FD-TD mode expanded results [2], [5], [7] can be used for further matrix operations or in conjunction with the mode-matching method. For such applications, we also need a method of wide-band $S$-parameter analysis, applicable to any practical case, including extraction of evanescent modes in a multimode environment at ports defined at inhomogeneously filled waveguides. It is also important to have a possibility of shifting the reference plane of the port in the post-processing stage of the FD-TD analysis and, thus, we need to know the propagation constant changes versus frequency at each of the ports.

Manuscript received September 2, 2002; revised December 5, 2002.

The authors are with the Instytut Radioelektroniki, Politechnika Warszawska, 00-665 Warsaw, Poland (e-mail: gwarek@ire.pw.edu.pl).

Digital Object Identifier 10.1109/TMTT.2003.815265

In the previously reported methods [2]–[5], the extraction of $S$-parameters is based on the assumption that, for each considered frequency and each considered mode of propagation in the port lines, we know the following:

- transverse-field distributions across the port line $\boldsymbol{e}_T(x,y)$ and $\boldsymbol{h}_T(x,y)$;
- relations between $\boldsymbol{e}_T(x,y)$ and $\boldsymbol{h}_T(x,y)$ in magnitude and phase (the mode impedance);
- propagation constant (magnitude and phase) of the mode.

In [2]–[4], it is assumed that the above relations are analytically known, which practically limits application to homogeneous guides. The method of [5] assumes that such information is extracted from a solution of a two-dimensional (2-D) eigenvalue problem. Such an approach works correctly for a single frequency. The lack of knowledge of the changes of the mode impedance and propagation constant versus frequency (which is a typical case of inhomogeneous guides) results in the eigenvalue problem solution needing to be repeated a large number of times. This makes the method computationally ineffective. Moreover, there are cases when the 2-D eigenvalue problem becomes difficult. We refer, for example, to the cases of lossy structures and/or solutions below the waveguide cutoff frequency.

This paper proposes a method in which we need to know the transverse-field distributions $\boldsymbol{e}_T(x,y)$ and $\boldsymbol{h}_T(x,y)$ to separate a particular mode, but we do not need to know *a priori* either the mode impedance or the propagation constant. Both are extracted from the three-dimensional (3-D) fields for each of the frequency points considered in $S$-parameter extraction. By such an approach, we eliminate the influence of the changes versus frequency of the mode impedance and the propagation constant. This makes the method in principle perfectly wide-band in the case of homogeneous guides—including the important practical case of lossy structures. In the case of inhomogeneous guides, some error appears due to the change of $\boldsymbol{e}_T(x,y)$ and $\boldsymbol{h}_T(x,y)$ with frequency. However, let us note that the changes in the transverse-field distributions $\boldsymbol{e}_T(x,y)$ and $\boldsymbol{h}_T(x,y)$ are usually much smaller than the changes in mode impedance or propagation constant (especially when we consider frequencies close to the waveguide cutoff). It is important to note that the changes of transverse-field distributions are quite small when the frequency drops below the waveguide cutoff and when we introduce losses. This makes it possible to accurately calculate the lossy cases with templates calculated for lossless equivalents and the evanescent mode cases with templates calculated above the cutoff frequency.

The application of our method to evanescent modes prompted us to consider some fundamental properties of the modes of nonreal mode impedance. As we will further show, such modes impose nontrivial questions on the very definition of the $S$-matrix, its properties, and its ability to explain physical phenomena in the circuit. These questions have not been formulated thus far by any of the papers on $S$-parameter extraction from time-domain simulations. They have been considered by Marks and Williams in their excellent theoretical paper [8]. However, while the authors of [8] concentrate on foundations for metrology applications, they put aside a theoretical case of evanescent modes in lossless circuits, which would impose in their theory several undefined values of parameters resulting from multiplication of zero by infinity. When considering $S$-parameter extraction from FD-TD analysis, we need to treat evanescent modes in lossless circuits as one of the basic cases. To have the theory fully applicable to this case, we need to modify some of the definitions proposed in [8].

## II. $S$-Matrix Definition and Mode Extraction

### A. Basic Issues in S-Matrix Definition

To investigate the behavior of the physical waves, let us consider a particular waveguide mode described by frequency-dependent complex amplitudes of transverse electric and magnetic fields

$$\boldsymbol{E}_T(x,y,z) = f_e(z)\boldsymbol{e}_T(x,y) \tag{1}$$

$$\boldsymbol{H}_T(x,y,z) = f_h(z)\boldsymbol{h}_T(x,y)\, e^{-j\varphi} \tag{2}$$

where

- $\boldsymbol{e}_T(x,y)$ and $\boldsymbol{h}_T(x,y)$ — real vector functions representing cross-sectional field patterns;
- $f_e(z)$ and $f_h(z)$ — complex scalar functions describing wave propagation along the considered transmission line;
- $\varphi$ — phase shift between electric and magnetic fields in a traveling wave.

In two typical situations, we have the following cases.

Case 1) In a purely traveling wave of amplitude $C_e$ in infinite waveguide

$$f_e(z) = C_e \mathrm{e}^{-\gamma z} \tag{3}$$

$$f_h(z) = C_h \mathrm{e}^{-\gamma z} \tag{4}$$

where $\gamma = \alpha + \mathrm{j}\beta$ is propagation constant of the considered mode.

Case 2) In the presence of reflections from the guide's end

$$f_e(z) = C_e(\mathrm{e}^{-\gamma z} + \Gamma \mathrm{e}^{\gamma z}) \tag{5}$$

$$f_h(z) = C_h(\mathrm{e}^{-\gamma z} - \Gamma \mathrm{e}^{\gamma z}) \tag{6}$$

where $\Gamma$ is the reflection coefficient.

In microwave engineering applications, it is often convenient to replace the field theory representation of waves in a transmission line (1), (2) by their circuit theory representation (7), (8)

$$U = U_0 f_e(z) \tag{7}$$

$$I = I_0 f_h(z) e^{-j\varphi} \tag{8}$$

where $U_0$ and $I_0$ are real scalars.

Voltage $U_0$ is the result of some integration over $\boldsymbol{e}_T(x,y)$ and current $I_0$ is the result of some integration over $\boldsymbol{h}_T(x,y)$. Only in the case of a pure TEM mode the extraction of $U_0$ from $\boldsymbol{e}_T(x,y)$ and $I_0$ from $\boldsymbol{h}_T(x,y)$ is unambiguous. In other cases, it is subject to specific (often application customized) definitions. Our proposals in this regard will be discussed further in this paper.

With $U_0$ and $I_0$ defined, we can also define the characteristic impedance of the transmission line

$$Z_{\mathrm{c}} = \frac{\mathrm{e}^{j\varphi} U_0}{I_0}. \tag{9}$$

The $S$-matrix describes relations between incident (denoted by $(a)$ and reflected $(b)$ waves. Therefore, to construct the $S$-matrix, we must answer the following two questions.

1) How to define the incident wave and reflected wave coefficients $a$ and $b$ as functions of $U$ and $I$?
2) How to extract $U_0$ and $I_0$ from $\boldsymbol{e}_T(x,y)$ and $\boldsymbol{h}_T(x,y)$?

We shall address these issues in Sections II-B and C.

### B. Definition of Incident and Reflected Waves

The answer to question 1) is clear as long as the incident and reflected waves at ports can be defined with respect to real reference impedance. In the case of nonreal impedance (and/or nonimaginary propagation constant), the physical incident and reflected waves are nonorthogonal. This means that the power transmitted to a port is not equal to the difference between the power flows calculated separately for the incident and reflected waves. A necessity to extend the $S$-matrix definition to such cases was noticed several decades ago, and a solution best known and used up to now was proposed by Kurokawa [10] as follows:

$$a_i = \frac{U_i + Z_{i\mathrm{ref}} I_i}{2\sqrt{|\mathrm{Re}(Z_{i\mathrm{ref}})|}} \tag{10}$$

$$b_i = \frac{U_i - Z^*_{i\mathrm{ref}} I_i}{2\sqrt{|\mathrm{Re}(Z_{i\mathrm{ref}})|}} \tag{11}$$

where

- $U_i$ and $I_i$ — mode voltages and currents at the $i$th port;
- $Z_{i\mathrm{ref}}$ — reference impedance at the $i$th port, which is, in principle, arbitrary, but the natural choice is making it equal to the characteristic impedance of the transmission line at this port $Z_{ic}$
- $*$ — denotes the complex conjugate.

Kurokawa's power waves defined with respect to nonreal $Z_{i\mathrm{ref}}$ are artificially orthogonalized, but as a result, they do not fulfil the Maxwell equations. To illustrate this point, let us choose $Z_{i\mathrm{ref}} = Z_{ic}$ and assume an evanescent mode with $Z_{ic}$ purely imaginary. From (10) and (11), we obtain $\Gamma_i = b_i/a_i \equiv 1$ irrespective of the physical situation, i.e., in both Case 1 (pure traveling wave) or Case 2 (partially standing wave) considered in Section II-A.

To construct a definition producing a physically relevant reflection coefficient, we need to assume

$$a_i = F(Z_{i\mathrm{ref}})(U_i + Z_{i\mathrm{ref}} I_i) \tag{12}$$

$$b_i = F(Z_{i\mathrm{ref}})(U_i - Z_{i\mathrm{ref}} I_i) \tag{13}$$

where $F$ is some arbitrary function of $Z_{i\mathrm{ref}}$ and its shape will be subject of the following discussion. Marks and Williams [8] propose that

$$F(Z_{i\mathrm{ref}}) = \frac{\sqrt{\mathrm{Re}(Z_{i\mathrm{ref}})}}{2|Z_{i\mathrm{ref}}|} \tag{14}$$

and call the obtained result "pseudo-waves" becoming "true waves" when $Z_{i\mathrm{ref}} = Z_{ic}$. They give a rationale for such a choice, which is fully convincing in metrology applications. However, when we consider evanescent waves in lossless guides, all the wave amplitudes due to (12)–(14) become zero. Thus, we should rather switch to other choices of $F(Z_{i\mathrm{ref}})$. In [9], we have used

$$F(Z_{i\mathrm{ref}}) = \frac{1}{2\sqrt{|Z_{i\mathrm{ref}}|}} \tag{15}$$

which is acceptable, but in the case of reciprocal circuits [see (37)], it assures only the condition of $|S_{ij}| = |S_{ji}|$. That is why, in this paper, we propose

$$F(Z_{i\mathrm{ref}}) = \frac{1}{2\sqrt{Z_{i\mathrm{ref}}}} \tag{16}$$

which, as we further show, assures a fully symmetrical $S$-matrix with $S_{ij} = S_{ji}$ for reciprocal circuits.

### C. Definition of Modal Voltages and Currents

With reference to (7) and (8), our aim now is to define two quantities representing amplitudes of the electric and magnetic fields of a particular mode, to be extracted from a multimode environment. It is only by analogy to TEM transmission lines that we shall call these two quantities "voltage" and "current" while they may be quite far away from the physical interpretations. A typical approach, e.g. [4], consists in calculating a scalar product (across the port) of the field $\boldsymbol{E}(x,y,t)$ obtained from the 3-D FD-TD simulation and the field $\boldsymbol{e}_{Ti}(x,y)$ of a pure $i$th mode (mode template) obtained analytically or from 2-D FD-TD eigenfunction analysis

$$U_i = \int_s \int \mathbf{E}(x,y,t) \cdot \mathbf{e}_{Ti}(x,y) ds \tag{17}$$

$$I_i = \int_s \int \boldsymbol{H}(x,y,t) \cdot \boldsymbol{h}_{Ti}(x,y) ds. \tag{18}$$

The approach described by (17), (18) is adequate for homogeneous waveguides. In the case of inhomogeneous waveguides it can be proven ([11, Ch. 10]) that the modes are not orthogonal with respect to scalar products like (17), and thus this approach does not separate the modes correctly. Among the quoted references only [5] and [8] use vector products applicable to inhomogeneous lines.

## III. The Proposed Method

We will now be considering the $i$th port of the investigated multiport. By "$i$th port," we understand an electromagnetic port associated with a particular mode of propagation. In the multimode environment, different electromagnetic ports can be associated with the same or different geometrical ports.

1) We propose that the mode voltages and currents be defined in the form of integrals across the port reference plane $z_p$ as follows:

$$U_i(t) = \int_s \int \boldsymbol{E}(x,y,z_p,t) \times \boldsymbol{h}_{Ti}(x,y,\omega_T) d\boldsymbol{s} \tag{19}$$

$$I_i(t) = \int_s \int \boldsymbol{e}_{Ti}(x,y,\omega_T) \times \boldsymbol{H}(x,y,z_p,t) d\boldsymbol{s} \tag{20}$$

where $\boldsymbol{e}_{Ti}(x,y,\omega_T)$ and $\boldsymbol{h}_{Ti}(x,y,\omega_T)$ are $E$- and $H$-field amplitudes of the $i$th-mode template at the frequency $\omega_T$, while

$$\int_s \int \boldsymbol{e}_{Ti}(x,y,\omega_T) \times \boldsymbol{h}_{Ti}(x,y,\omega_T) d\boldsymbol{s} = 1. \tag{21}$$

The mode templates are obtained from 2-D FD-TD calculations, e.g., using the method proposed in [12]. Transverse-field distributions $\boldsymbol{e}_{Ti}(x,y,\omega_T)$ and $\boldsymbol{h}_{Ti}(x,y,\omega_T)$ are real functions and, thus, do not contain the information about possible phase difference between the fields. This information is available in $\boldsymbol{E}(x,y,z_p,t)$ and $\boldsymbol{H}(x,y,z_p,t)$ and will be further extracted in a procedure described by (22)–(30). Thus, the method is also applicable to lossy structures as long as the mode fields can be expressed in the form described by (1) and (2).

2) Based upon the discussion in Section II, we propose the following definition of the incident and reflected waves:

$$a_i(\omega) = \frac{U_i(\omega) + Z_i(\omega) I_i(\omega)}{2\sqrt{Z_i(\omega)}} \tag{22}$$

$$b_i(\omega) = \frac{U_i(\omega) - Z_i(\omega) I_i(\omega)}{2\sqrt{Z_i(\omega)}} \tag{23}$$

with $Z_i(\omega) = Z_{ic}(\omega)$ being the mode impedance equal to the ratio of the mode voltage and current in the reflectionless case (9). Let us note that following (19)–(21), at the frequency $\omega_T$, the mode impedance of the $i$th mode is

$$\mathrm{Z}_i(\omega) = e^{j\varphi}. \tag{24}$$

Equations (22) and (23) impose

$$U_i(\omega) = \big(a_i(\omega) + b_i(\omega)\big)\sqrt{\mathrm{Z_i}(\omega)} \tag{25}$$

$$I_i(\omega) = \frac{\big(a_i(\omega) - b_i(\omega)\big)}{\sqrt{\mathrm{Z_i}(\omega)}}. \tag{26}$$

Unlike Kurokawa's definitions, those presented above are consistent with Maxwell's equations. For example, they ensure zero reflection coefficient in an infinitely long waveguide, also below the cutoff frequency of the considered mode.

3) The $S$-matrix is extracted by an extension of the differential method originally reported in [13]. From the port reference

plane fields, we calculate the values of

$$\begin{aligned} U_i(\omega) &= F\{U_i(t)\} \\ I_i(\omega) &= F\{I_i(t)\} \end{aligned} \tag{27}$$

$$\begin{aligned} U_i'(\omega) &= F\left\{\frac{\partial U_i(z,t)}{\partial z}\right\} \\ I_i'(\omega) &= F\left\{\frac{\partial I_i(z,t)}{\partial z}\right\} \end{aligned} \tag{28}$$

for each $i$th mode, where $F$ denotes the Fourier transform.

Using the quantities specified in (27) and (28) and following the rules of the differential method [13], we can extract

$$Z_i(\omega) = \sqrt{\frac{U_i(\omega)U_i'(\omega)}{I_i(\omega)I_i'(\omega)}} \tag{29}$$

and then the values of $a_i(\omega)$ and $b_i(\omega)$ with the relations (22) and (23). The quantities of (27) and (28) also produce the propagation constant at the $i$th port as follows:

$$\gamma_i(\omega) = \alpha_i(\omega) + j\beta_i(\omega) = \sqrt{\frac{I_i'(\omega)U_i'(\omega)}{I_i(\omega)U_i(\omega)}}. \tag{30}$$

Equations (27)–(30) allow wide-band extraction of the $S$-matrix with compensation for imperfect matching of the loads. Frequency dependence of the reference (modal) impedances is automatically taken into account. Moreover, the information of (30) can also be used for a virtual shift of the port reference planes at the post-processing stage. The knowledge of the propagation constant allows us to extract the derivatives of (28) more accurately than by standard finite differencing. For the case of propagating modes (imaginary propagation constant), the relevant formula can be found in [13]. For the case of evanescent modes (real propagation constant), the formula (e.g., voltage derivative) becomes

$$\frac{\partial U_i(z,t)}{\partial z} = \frac{U_i\left(z+\frac{\Delta z}{2},t\right) - U_i\left(z-\frac{\Delta z}{2},t\right)}{\Delta z}\frac{\alpha\Delta z}{\sinh(\alpha\Delta z)}. \tag{31}$$

At first, the derivatives of (28) are calculated by standard finite differencing of the FD-TD fields and are used to extract the propagation constant from (30). We then apply (31) to recalculate the derivatives with enhanced accuracy. Such an approach is formally iterative, but practically converges after one iteration.

## IV. Properties of the Obtained $S$-Matrices

Our system described by 3) in Section III uses a "natural" definition of the $S$-matrix with the reference impedance $Z_i(\omega)$ equal to the ratio of the mode voltage and current in a reflectionless case (9). This allows an easy shift of the reference plane by $\Delta l$ through a simple multiplication of the waves $a_i(\omega)$ and $b_i(\omega)$ by factors $e^{\pm\gamma\Delta l}$ with the value of $\gamma$ extracted by (30). Yet we must note that this choice of the $S$-matrix definition imposes complex or even purely imaginary values of the reference impedance $Z_i(\omega)$ in some practical cases. Segments of a microwave circuit described by so-defined $S$-matrices can be subject to cascading /de-cascading (or embedding/deembedding) operations basically the same way, regardless of the reference impedance being real, imaginary, or complex. However, with nonreal reference impedances, the $S$-matrices have different properties than with the real ones. Most interesting of these properties will be investigated here.

### A. Real Power Transmitted to a Guide Port

Let us calculate the real power transmitted to a waveguide port with the input reflection coefficient $\Gamma_i = b_i/a_i$. Using (25) and (26), we obtain

$$P_i = \mathrm{Re}(U_i I_i^*) = \mathrm{Re}\Big(|a_i|^2\big(1-|\Gamma_i|^2+\mathrm{j}2\,\mathrm{Im}(\Gamma_i)\big)e^{j\varphi}\Big). \tag{32}$$

For a propagating mode in a lossless structure, the impedance $Z_i$ is real, which imposes $\varphi = 0$ and a well-known result as follows:

$$P_i = |a_i|^2\left(1 - |\Gamma_i|^2\right). \tag{33}$$

For an evanescent mode, the impedance $Z_i$ is imaginary, which imposes $\varphi = \pm\pi/2$ and

$$P_i = \mp|a_i|^2\big(2\,\mathrm{Im}(\Gamma_i)\big). \tag{34}$$

The above result seems unintuitive, but a closer look reveals its physical sense. With an infinite guide, the reflection coefficient is equal zero and there is no real power flow. Also, reactive impedance termination does not cause any real power flow because the corresponding $\Gamma_i$ is real. However, a resistive termination of an evanescent mode causes power dissipation in the load and, thus, also a real power transmission through the guide. Such power transmission is predicted by (34) because the resistive termination imposes a nonzero imaginary part of $\Gamma_i$.

### B. Reciprocity Relations

Let us consider two different solutions of Maxwell equations marked with $^a$ and $^b$, which produce the known reciprocity relation

$$\int_s\int (\boldsymbol{E}^a \times \boldsymbol{H}^b - \boldsymbol{E}^b \times \boldsymbol{H}^a)d\boldsymbol{s} = 0. \tag{35}$$

We will apply (35) to the case of a multiport with just two ports $i$ and $j$ involved in the integration of (35) and all other ports perfectly matched inside the surface of integration. Applying the relations (19) and (20), we obtain

$$U_i^a I_i^b + U_j^a I_j^b - U_i^b I_i^a - U_j^b I_j^a = 0. \tag{36}$$

Now we replace the values of $U$ and $I$ by the incident and reflected waves following (12) and (13). We assume that, in the case $^a$, the $j$th port is perfectly matched, while in the case $^b$, the $i$th port is perfectly matched. This assumption imposes $a_j^a = 0$

and $a_i^b = 0$ and transformation of the formulas leads to the relation

$$\frac{b_i^b}{a_j^b}\frac{Z_{j\mathrm{ref}}F^2(Z_{j\mathrm{ref}})}{Z_{i\mathrm{ref}}F^2(Z_{i\mathrm{ref}})} = \frac{b_j^a}{a_i^a}. \tag{37}$$

Equation (37) justifies the choice of $F(Z_{\mathrm{ref}})$, as in (16), which produces a fully symmetrical $S$-matrix with $S_{ij} = S_{ji}$ for any reference impedances at ports.

### C. Power Balance Relations in a Lossless Multiport

The following relation is well known in the case of a lossless multiport with real reference impedances:

$$\sum_{j=1}^{n} |s_{ji}|^2 = 1. \tag{38}$$

Let us examine how this relation will be transformed if we allow imaginary reference impedance at some of the ports. We need to distinguish two cases concerning the input ($i$th) port. In the first case, we assume that $Z_i$ is real and we obtain the result similar to (38), but eliminating from the summation all those $S_{ji}$ to outputs $j$, where $Z_j$ is imaginary. In the second case, we assume imaginary $Z_i$ at the input and obtain

$$\mp 2\,\mathrm{Im}(S_{ii}) = \sum_j |S_{ji}|^2 \tag{39}$$

with the summation extended exclusively over those outputs where $Z_j$ is real and the $\mp$ sign is the reverse of the sign in the $\pm j$ phase angle of $Z_j$.

### D. Special Case of a Reciprocal Lossless Two-Port

In the classical approach with real reference impedances, the reciprocity relation combined with power balance additionally produces the following well-known conditions:

$$|S_{11}| = |S_{22}| \tag{40}$$

$$\mathrm{Arg}(S_{11}) + \mathrm{Arg}(S_{22}) - 2\,\mathrm{Arg}(S_{21}) = \pm\pi. \tag{41}$$

The relations (40) and (41) are practically important in electromagnetic simulations because they allow extracting a full $S$-matrix of a lossless two-port after just one excitation from one of the ports. Let us now try to derive analogous relations in the case when $Z_1$ is real, but $Z_2$ is imaginary.

Power balance relations (38) and (39) and reciprocity (37) immediately give

$$|S_{11}| = 1 \tag{42}$$

$$\mp 2\,\mathrm{Im}(S_{22}) = |S_{21}|^2 = |S_{12}|^2. \tag{43}$$

To find a condition replacing (41), let us consider input reflection coefficient $\Gamma_2$ with the input placed at port 2 when the output (port 1) is terminated with a reflection coefficient $\Gamma_1$. Simple operations on the $S$-matrix elements give

$$\Gamma_2 = S_{22} + \frac{S_{12}S_{21}}{S_{11}\left(\frac{1}{\Gamma_1 S_{11}} - 1\right)}. \tag{44}$$

According to (34), the total reflection at port 1 ($|\Gamma_1| = 1$) should produce purely real $\Gamma_2$. Thus, we can write

$$\mathrm{Im}(S_{22}) = \mathrm{Im}\left(\frac{-S_{12}S_{21}}{S_{11}\left(\frac{1}{\Gamma_1 S_{11}} - 1\right)}\right). \tag{45}$$

Taking into account that

$$|S_{11}| = 1$$
$$|\Gamma_1| = 1$$
$$2\mathrm{Im}(S_{22}) = |S_{21}S_{12}|$$
$$\mathrm{Re}\left(\frac{1}{(e^{j\alpha} - 1)}\right) = -0.5 \text{ for arbitrary } \alpha$$

and also that (45) needs to be obeyed for $\Gamma_1$ of the arbitrary phase angle, we obtain the phase condition

$$\mathrm{Arg}(S_{11}) - \mathrm{Arg}(S_{21}) - \mathrm{Arg}(S_{12}) = \pm\frac{\pi}{2} \tag{46}$$

with the sign $\pm$ equal to the sign in the $\pm j$ phase angle of $Z_2$.

Conditions (42), (43), and (46) provide interesting practical information. We can extract the entire $S$-matrix of a lossless reciprocal two-port based on $S_{22}$ and $S_{12}$ obtained from just one simulation with excitation at port 2 (of imaginary $Z_2$) and matched or quasi-matched conditions at port 1 (of real $Z_1$). However, we cannot extract the entire $S$-matrix in one simulation with excitation at port 1. In such a case, it does not seem possible to reproduce the real part of $S_{22}$.

## V. Software Implementation and Examples of Analysis

The method described in this paper has been implemented by the authors in the FD-TD *QuickWave-3D* v.2.1 simulator [14]. Operations on $S$-matrices describing circuit segments have been performed with the $S$-matrix converting module [15].

*Example 1:* Let us consider a segment of a rectangular waveguide with 10 mm$\times$ 5 mm cross section, short circuited at the end. We assume that the waveguide is filled with a medium having the permittivity and permeability of vacuum, but with the conductivity of $\sigma = 0.15[1/(\Omega\mathrm{m})]$. Reflection coefficient has been extracted at a reference plane located at a distance of 15 mm from the short with a uniform FD-TD mesh of 0.5 mm. The template of the dominant mode at 22.5 GHz has been used over the entire frequency range. The simulation results are presented in Fig. 1 in the form of continuous lines—the black line denoting the magnitude and the grey line denotes the phase. It can be seen that, above the cutoff frequency (15 GHz), we have the propagating wave region with fast phase changes and slow magnitude changes, while below 15 GHz, we have the evanescent wave region with slow changes of the phase. At the same time, the magnitude decreases quickly to very low values (approximately $-60$ dB for 10 GHz).

At the post-processing stage, the reference plane has been virtually shifted to the position of the short termination, using the complex propagation constant extracted by the differential method (30). The results are presented in Fig. 1 as dotted horizontal lines (the black line at 0 dB for the magnitude and the

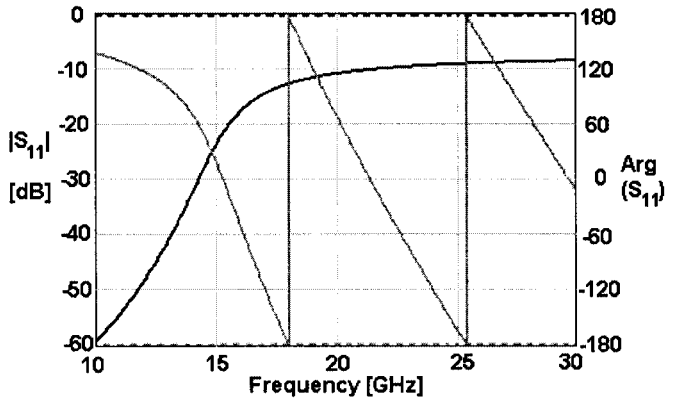


Fig. 1. Magnitude (black lines) and phase (grey lines) of the reflection coefficient versus frequency in a short-circuited lossy waveguide section extracted directly from FD-TD simulations at 15 mm from the back wall (continuous lines) and calculated with a virtual shift of the reference plane to the back wall (dotted horizontal lines at 0 dB for magnitude and $-180°$ for phase).

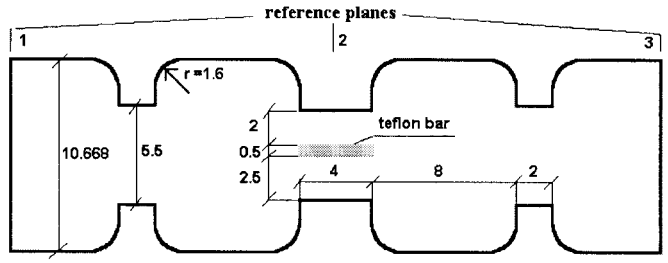


Fig. 2. Shape of the considered two-resonator waveguide $H$-plane filter with a Teflon bar in the center. All dimensions are in millimeters.

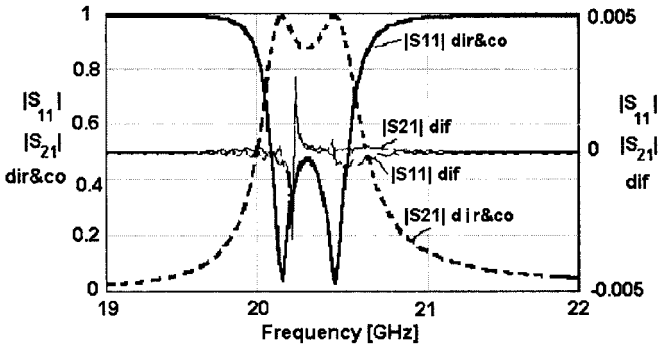


Fig. 3. $S$-parameters obtained from the FD-TD analysis of the filter of Fig. 2 calculated directly (dir), combined from the parameters of two halves presented in Fig. 2 (co), and the difference between the above results shown in expanded scale.

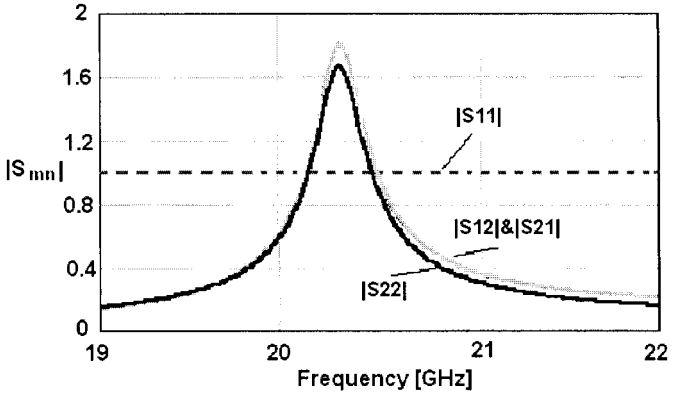


Fig. 4. Magnitudes of $S$-parameters of one-half of the filter of Fig. 2 calculated with a propagating mode at the input (reference plane 1) and an evanescent mode at the output (reference plane 2).

grey line at $-180°$ for the phase). We can add that the anticipated values of $|S_{11}| = 0$ dB and $< S_{11} = \pm 180°$ have been obtained in the entire frequency band with an impressive accuracy. The maximum magnitude error is approximately 0.001 dB, while the maximum phase error is approximately 0.03°.

*Example 2:* We now consider a two-resonator $H$-plane filter in rectangular waveguide technology, as presented in Fig. 2. The structure is air filled, except for a Teflon bar in the coupling area between the resonators. Moving the bar closer to the waveguide center increases the coupling between the resonators and, thus, deepens a ripple in the center of the filter characteristics of Fig. 3. The side position of the bar produces a maximally flat filter characteristic.

We compare the results extracted directly from the FD-TD analysis of the entire structure (between reference planes 1 and 3 in Fig. 2) and combined by cascading the $S$-matrices of the two halves of the structure (between planes 1 and 2 and planes 2 and 3). Please note that, by virtue of symmetry, in the latter case, only one-half of the structure needs to be simulated by FD-TD. The results are presented in Fig. 3. The differences between the two approaches are displayed on the separate amplified scale because they are extremely small (an order of 0.002).

It is also very interesting to look at the $S$-parameters of one-half of the circuit (planes 1 and 2), presented in Figs. 4 and 5. In Fig. 4, we can see that $|S_{11}| = 1$, as expected from (42). Absolute values of the remaining three $S$-parameters show resonant character and, in a certain frequency range, exceed unity. Although surprising at first sight, this is consistent with the properties of the generalized $S$-matrices discussed in Section IV. Confirming the reciprocity relations of Section IV, we also find that $S_{12} = S_{21}$ in both magnitude and phase. Moreover, it can be shown that both conditions (43) and (46) are obeyed with high accuracy. In this example, we have phase angle of the reference impedance at port 2 equal to $+\pi/2$, which (according to (43)) produces a purely negative imaginary part of $S_{22}$ or, in other words, the phase of $S_{22}$ between 0 and $-\pi$. However, the most important proof of physical consistency of the results presented in Fig. 4 and Fig. 5 is the fact that their cascading produces the correct full filter characteristics of Fig. 3.

*Example 3:* We consider another waveguide $H$-plane filter with the long section presented in Fig. 6. The waveguide is 5-mm wide and, at the filter input and output, we have a ceramic insert of relative permittivity 9.7, 1-mm wide. Inside the guide, we have two dielectric resonators of relative permittivity 7, dimensions 2 mm $\times$ 1 mm. The ceramic inserts and resonators span the full height of the guide. This structure will be used to test $S$-parameter extraction in a very wide band—from 10 to 50 GHz.

The structure of Fig. 6 can be considered as a combination of six step junctions between air-filled waveguide and partially dielectric-filled waveguide (four with permittivity equal seven and two with permittivity equal 9.7). Thus, we have calculated

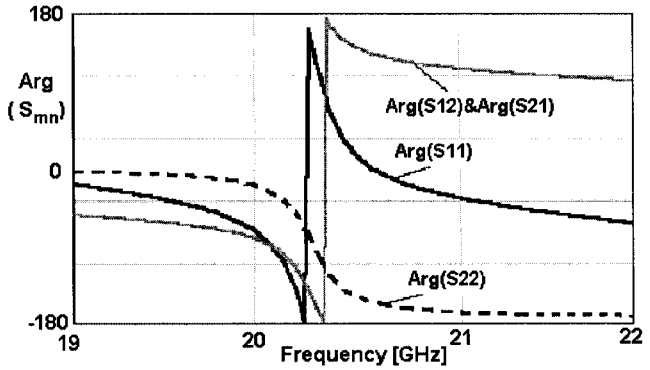


Fig. 5. Phase angles of $S$-parameters of one-half of the filter of Fig. 2 calculated with a propagating mode at the input (reference plane 1) and an evanescent mode at the output (reference plane 2).

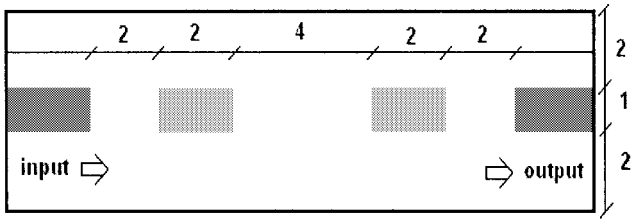


Fig. 6. Long section of the waveguide filter considered in Example 3, with dimensions in millimeters.

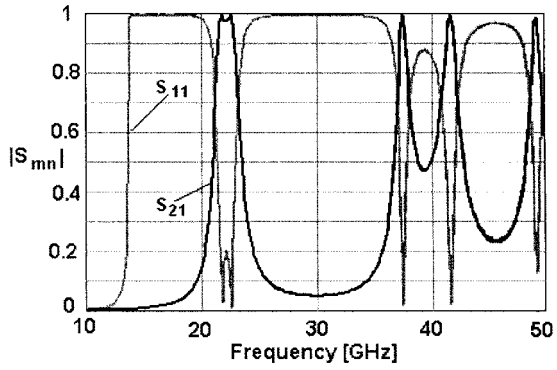


Fig. 7. Magnitudes of $S$-parameters $|S_{11}|\&|S_{21}|$ of the structure of Fig. 6 calculated directly and by matrix operations on the six individual discontinuities. Curves in both cases practically coincide.

the structure response first directly from FD-TD simulation, and then by matrix operations on $S$-matrices of the six discontinuities. In the latter case, only two FD-TD simulations of small nonresonant discontinuities have been necessary, making the analysis much faster than in the case of the entire resonant structure. All modal templates have been calculated at 25 GHz.

Fig. 7 presents the curves obtained directly and by cascading of the six discontinuities. Results for both cases are practically the same. It can be added (which is not shown in Fig. 7) that, in each case, the relations $|S_{11}| = S_{22}|$ and $|S_{21}| = |S_{12}|$ are also obeyed with very high accuracy.

However, it should be admitted that such a good result is partially due to a symmetrical character of the structure helping to compensate errors of calculation. Let us look at Fig. 8, which shows the results of extraction of $|S_{12}|$ and $|S_{21}|$ from a single input discontinuity of the structure of Fig. 6 (a step between an

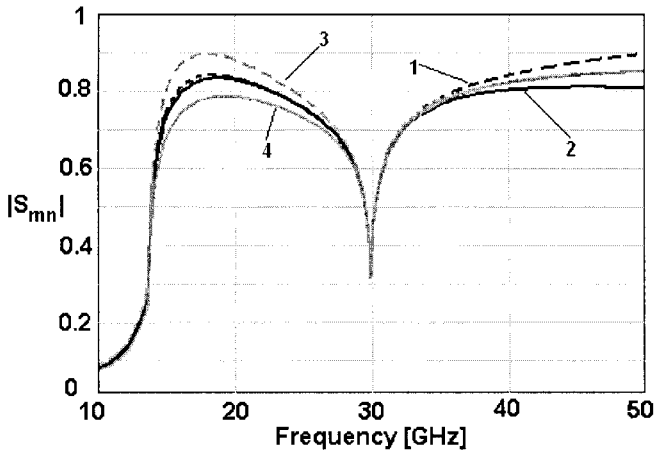


Fig. 8. Magnitudes of $S$-parameters $|S_{21}|$ (curves 1 and 3) and $|S_{12}|$ (curves 2 and 4) for a single-input discontinuity of the structure of Fig. 6, with the mode templates calculated at 25 GHz (curves 1 and 2) and with the mode templates calculated at 42 GHz (curves 3 and 4).

air-filled guide and a guide with a ceramic insert). These results are a part of those used for calculation of the result of Fig. 7 as a combination of the six discontinuities. A single discontinuity is highly asymmetrical and, thus, the calculation errors appear mostly as a difference between $|S_{12}|$ and $|S_{21}|$. From Fig. 8, it can be seen that, with the mode templates calculated at 25 GHz, the curves of $|S_{12}|$ and $|S_{21}|$ diverge above 35 GHz, indicating a visible error of analysis for the upper part of the band. This error can be eliminated by using a mode template calculated at 42 GHz (curves 3 and 4). However, in such a case, the analysis at lower frequencies is somewhat less accurate. A simple remedy to such an error is enforcing the reciprocity by admitting that both $|S_{12}|$ and $|S_{21}|$ are equal to the average between them. It can be verified that, in the case of Fig. 8, the results obtained this way with each of the templates are practically the same all over the frequency band.

Example 3 concerns a situation of an extremely wide frequency band and very big differences in the dispersion properties of the input and output guides. Under such circumstances, we may have doubts if using just one template for each port will give sufficient accuracy in the entire frequency band. Such doubts can be relatively easily clarified. We can calculate two templates for each port, one of them close to the upper limit and the other one close to the lower limit of the considered frequency band. During the 3-D FD-TD simulation, we can calculate two sets of the $S$-parameters with the two sets of templates. Projecting such obtained $S$-parameter curves on the same scale immediately reveals if (and by how much) they diverge due to the template change. We can thus verify which parts of the curves of $S$-parameters versus frequency are fully reliable. Such an approach has been implemented in our software and has been proven practical. Its application typically increases the total computing time and memory not more than by a few percent.

*Example 4:* We consider a spiral inductor with an air bridge first presented in [16] and then used as a benchmark by other authors. We assume all dimensions of the structure as in [16]. Fig. 9 shows the comparison of three curves

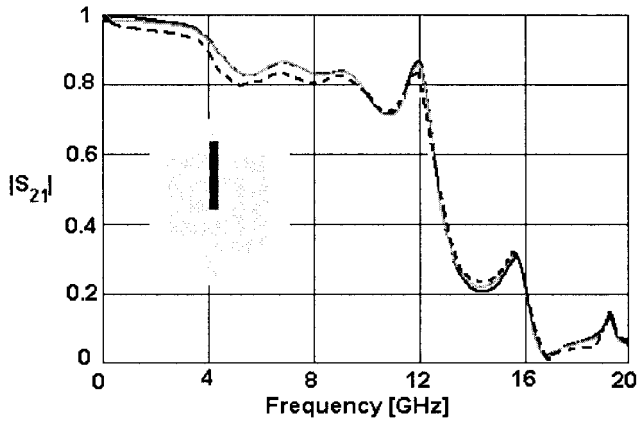


Fig. 9. Magnitude of $S_{21}$ of the spiral inductor considered originally in [16]. Continuous curves (with a negligible differences between them) show the results of simulation by our method assuming a mode template calculated at one frequency—2 GHz (black line) and 18 GHz (grey line). Dotted line presents the results of measurements after [16].

- our calculations with a template at 2 GHz (black line);
- our calculations with a template at 18 GHz (grey line);
- measurements after [16] (black dotted line).

The agreement between the simulations and measurements is very good. The only visible difference is that the measured magnitude of $S_{21}$ is at lower frequencies approximately 0.2 dB lower than the simulated one. Since a similar shift of magnitude was obtained in simulations performed by the authors of [16], it is quite reasonable to assume that it is due to the measurement's setup calibration error or some small series resistance introduced by the applied technology of circuit fabrication. Let us note that the differences between the two curves obtained with the two templates are negligible, which indicates that, in this case, the $S$-parameters can be extracted accurately wide band with a single template.

## VI. Conclusions

The proposed method of $S$-parameter extraction proves to be very versatile, accurate, and effective in practical applications. A combination of those properties permits to compare it favorably versus the previously reported methods. The following is worth noting.

- It has proven applicable to frequency bands above and below cutoff frequencies of transmission lines.
- In the examples, we have considered only one mode at each port, but the mode-filtering properties described by (19) and (20) make the method fully applicable to a multimode environment. This has been verified in the simulation practice.
- In all the presented examples, it has been possible to extract accurate wide-band results with mode templates calculated at a single frequency. This is due to wide-band properties of the differential method, which extracts and automatically takes into account the frequency-dependent behavior of the modal impedance and propagation constant.
- The method cannot fully compensate for the errors due to the frequency-dependent changes of the transverse-field distributions $\boldsymbol{e}_{Ti}(x,y,\omega)$ and $\boldsymbol{h}_{Ti}(x,y,\omega)$ in inhomogeneous guides. Such errors are usually quite small. However, in the case of wide-band simulation of inhomogeneous guides, it is advisable to verify their level by comparing the $S$-parameters obtained with mode templates calculated at two or three different frequencies. Such a procedure has been implemented by the authors and proven relatively inexpensive in terms of computer time and memory.
- The method is applicable to lossy structures as long as the fields can be expressed in the form of (1) and (2). These assumptions are not rigorously met in the case of inhomogeneous lossy transmission lines. However, the authors experience shows that the method can be applied with good accuracy to practical low-loss inhomogeneous lines with $\boldsymbol{e}_t(x,y)$ and $\boldsymbol{h}_t(x,y)$ generated for a corresponding lossless line.
- Applicability of the proposed method to cases where the assumptions given by (1) and (2) cannot be made (as, e.g., complex modes) should be a subject of a separate study.

## Acknowledgment

The authors wish to acknowledge the assistance in preparation of this paper of the other main coauthors of the *QuickWave-3D* software, i.e., Dr. M. Sypniewski and Dr. A. Wieckowski, both of QWED Company, Warsaw, Poland.

## References

[1] W. K. Gwarek, "Analysis of arbitrarily shaped two-dimensional microwave circuits by finite-difference time-domain method," *IEEE Trans. Microwave Theory Tech.*, vol. 36, pp. 738–744, Apr. 1988.

[2] T. Shibata and T. Itoh, "Generalized-scattering-matrix modeling of waveguide circuits using FDTD field simulations," *IEEE Trans. Microwave Theory Tech.*, vol. 46, pp. 1742–1751, Nov. 1998.

[3] A. Kreczkowski and M. Mrozowski, "Multimode analysis of waveguide discontinuities using the concept of generalized scattering matrix and power waves," in *Proc. 13th Int. MIKON Conf.*, Wroclaw, Poland, May 2000, pp. 569–572.

[4] E. Navarro, T. Bordallo, and J. Navasquillo-Miralles, "FDTD characterization of evanescent modes—multimode analysis of waveguide discontinuities," *IEEE Trans. Microwave Theory Tech.*, vol. 48, pp. 606–610, Apr. 2000.

[5] J. Ritter and F. Arndt, "Efficient FDTD/matrix pencil method for full-wave scattering parameter analysis of waveguiding structures," *IEEE Trans. Microwave Theory Tech.*, vol. 44, pp. 2450–2456, Dec. 1996.

[6] M. Righi, W. Hoefer, M. Mongiardo, and R. Sorrentino, "Efficient TLM diakoptics for separable structures," *IEEE Trans. Microwave Theory Tech.*, vol. 43, pp. 854–859, Apr. 1995.

[7] F. Alimenti, P. Mezanotte, L. Roselli, and R. Sorrentino, "Analysis of planar circuits with a combined 3-D FDTD-time domain modal expansion method," in *IEEE MTT-S Int. Microwave Symp. Dig.*, San Francisco, CA, June 1996, pp. 1471–1474.

[8] R. B. Marks and D. F. Williams, "A general waveguide circuit theory," *J. Res. Nat. Inst. Standards Technol.*, vol. 97, no. 5, pp. 533–562, Sept.–Oct. 1992.

[9] W. K. Gwarek and M. Celuch-Marcysiak, "A generalized approach to wide-band $S$-parameter extraction from FD-TD simulations applicable to evanescent modes in inhomogeneous guides," in *IEEE MTT-S Int. Microwave Symp. Dig.*, Phoenix, AZ, 2001, pp. 885–888.

[10] K. Kurokawa, *An Introduction to the Theory of Microwave Circuits*. New York: Academic, 1969.

[11] M. Mrozowski, *Guided Electromagnetic Waves-Properties and Analysis*. Taunton, MA: Res. Studies Press, 1997.
[12] W. K. Gwarek, T. Morawski, and C. Mroczkowski, "Application of the FD-TD method to the analysis of circuits described by the two-dimensional vector wave equation," *IEEE Trans. Microwave Theory Tech.*, vol. 41, pp. 311–317, Feb. 1993.
[13] W. K. Gwarek and M. Celuch-Marcysiak, "A differential method of reflection coefficient extraction from FD-TD simulations," *IEEE Microwave Guided Wave Lett.*, vol. 6, pp. 215–217, May 1996.
[14] *QuickWave-3D User's Manual*, *v.2.1*, QWED Company, Warsaw, Poland, 2002.
[15] T. Ciamulski, "Program for analysis of multiport microwave structures," M.S. thesis (in Polish), Warsaw Univ. Technol., Warsaw, Poland, 2000.
[16] T. Becks and I. Wolff, "Analysis of 3-D metallization structures by a full-wave spectral domain technique," *IEEE Trans. Microwave Theory Tech.*, vol. 40, pp. 2219–2227, Dec. 1992.

**Wojciech K. Gwarek** (SM'90–F'01) was born in Poland. He graduated from the Warsaw University of Technology, Warsaw, Poland, in 1970. He received the M.Sc. degree from the Massachusetts Institute of Technology (MIT), Cambridge, in 1974 and the Ph.D. degree from the Warsaw University of Technology, in 1977.

He is currently a Professor with the Warsaw University of Technology. His early research activity concentrated on nonlinear analysis of microwave mixers and measurements. Since the mid-1980s, he has been engaged in research on electromagnetic analysis in time domain. Since 1990, his activity also has included the development of commercial software tools by himself and a group of his co-workers. The brand names of these tools, i.e., *QuickWave* and *Concerto*, have become popular worldwide. He is the founder and President of the QWED Company, Warsaw, Poland, which successfully commercializes these tools.

Dr. Gwarek has been involved in many IEEE activities as a reviewer for various publications and as a member of the Technical Program Committee (TPC) of the IEEE Microwave Theory and Techniques Society International Microwave Symposium (IEEE MTT-S IMS) and the chairman of the MTT/Antennas and Propagation (AP)/Aerospace and Electronics Systems (AES) Joint Chapter of Poland.

**Malgorzata Celuch-Marcysiak** (M'97) received the International Baccalaureate degree from the United World College of the Atlantic, Wales, U.K., in 1983, and the M.Sc. and Ph.D. degrees in electronic engineering from the Warsaw University of Technology, Warsaw, Poland, in 1988 and 1996, respectively.

She is currently an Assistant Professor with the Warsaw University of Technology. She is one of the main authors of the electromagnetic simulation software *QuickWave* and *Concerto* and also co-founder and vice-president of the QWED Company, Warsaw, Poland, which commercializes these tools. She has contributed to over 60 technical publications. Her main professional interest is in numerical modeling of electromagnetic problems.

Dr. Celuch-Marcysiak has acted as reviewer for the IEEE TRANSACTIONS ON MICROWAVE THEORY AND TECHNIQUES, the IEEE TRANSACTIONS ON ANTENNAS AND PROPAGATION, and IEEE MICROWAVE AND WIRELESS COMPONENTS LETTERS. She has been a member of the Technical Program Committee (TPC) of the IEEE Microwave Theory and Techniques Society International Microwave Symposium (IEEE MTT-S IMS).